Assimilating Surface Data to Improve the Accuracy of Atmospheric Boundary Layer Simulations

KIRAN ALAPATY

MCNC-Environmental Programs, Research Triangle Park, North Carolina

NELSON L. SEAMAN

Department of Meteorology, The Pennsylvania State University, University Park, Pennsylvania

DEVDUTTA S. NIYOGI

Department of Marine, Earth, and Atmospheric Sciences, North Carolina State University, Raleigh, North Carolina

ADEL F. HANNA

MCNC-Environmental Programs, Research Triangle Park, North Carolina

(Manuscript received 13 April 2000, in final form 18 April 2001)

ABSTRACT

Large errors in atmospheric boundary layer (ABL) simulations can be caused by inaccuracies in the specification of surface characteristics in addition to assumptions and simplifications made in boundary layer formulations or other model deficiencies. For certain applications, such as air quality studies, these errors can have significant effects. To reduce such errors, a continuous surface data assimilation technique is developed. In this technique, surface-layer temperature and water vapor mixing ratio are directly assimilated by using the analyzed surface data. Then, the difference between the observations and model results is used to calculate adjustments to the surface fluxes of sensible and latent heat. These adjustments are then used to calculate a new estimate of the ground temperature, thereby affecting the simulated surface fluxes on the subsequent time step. This indirect data assimilation is applied simultaneously with the direct assimilation of surface data in the model's lowest layer, thereby maintaining greater consistency between the ground temperature and the surface-layer mass-field variables. A one-dimensional model was used to study the improvements that result from applying this technique for ABL simulations in two cases. It was found that application of the new technique led to significant reductions in ABL modeling errors.

1. Introduction

The accuracy of modeled atmospheric boundary layer (ABL) structure critically depends on 1) the accuracy of initial conditions and specified surface parameters, 2) the kind of formulation used to represent surface and turbulent processes, 3) the spatial resolution of the model, and 4) the effective simulation of mesoscale and large-scale dynamics. A large number of studies (e.g., Pleim and Xiu 1995; Sistla et al. 1996; Alapaty et al. 1997b; Alapaty and Mathur 1998; Niyogi et al. 1999; Russell and Dennis 2000) have confirmed that ABL modeling errors can arise from one or more of these factors. Also, several of these studies found that such errors can have damaging effects in subsequent air pollution modeling (Sistla et al. 1996; Alapaty and Mathur 1998; Russell and Dennis 2000).

To alleviate such simulation errors, Ruggiero et al. (1996) have studied the effects of frequent assimilation of surface observations using an objective analysis in an intermittent technique. They found that their simple intermittent data assimilation improved mesoscale analyses and forecasts. However, intermittent assimilation can lead to dynamic imbalances and mass inconsistencies each time the model is restarted, which is undesirable for certain applications such as air quality studies (Seaman 2000). Stauffer et al. (1991) studied the impacts of direct assimilation of surface temperature observations in a continuous four-dimensional data assimilation (FDDA). They found that this approach reduces surface temperature errors but can lead to serious errors

Corresponding author address: Dr. Kiran Alapaty, MCNC-Environmental Programs, P.O. Box 12889, 3021 Cornwallis Road, Research Triangle Park, NC 27709-2889.
E-mail: alapaty@ncsc.org

in ABL structure because the sign of the surface buoyancy flux can change unrealistically as new data are assimilated, even in midday conditions. Lohmann et al. (1999) recently performed 1D simulations using a simple relaxation assimilation technique to improve their model simulations. A disadvantage in their method is the uncertainty in specifying the relaxation timescale. Despite progress in reducing errors associated with each of these factors, it remains difficult to prevent significant errors in all cases. For these reasons, there is a need to develop better data assimilation techniques for thermodynamic variables to alleviate prediction errors in the ABL further.

In recent years, much attention has been given to improving ABL predictions by addressing the surface boundary conditions used in atmospheric models. For a given synoptic condition, the ABL structure and evolution are controlled through both the entrainment fluxes at the top of the ABL and by surface fluxes, but primarily through the latter. Thus, multilevel soil models, some with vegetative canopy submodels (e.g., Noilhan and Planton 1989), have become more common and have been coupled with rainfall estimates to provide case-specific soil-moisture profiles (e.g., Chen et al. 1996, 1997; Chen and Dudhia 2001). However, this approach relies heavily on the accuracy of the land surface models and rain estimates, which are often taken from prior forecast-model runs. Mahfouf (1991) and Bouttier et al. (1993) used the evolving surface-layer temperature and humidity to estimate the soil moisture in numerical model predictions. McNider et al. (1994) took a similar approach, but assimilated satellite-observed surface skin temperature tendencies to estimate soil moisture. These techniques work well, but they assume that the largest errors in the simulated surface-energy budget are due to errors in the soil moisture parameter, which may not always be true, especially if there are also cloud prediction errors. Ruggiero et al. (2000) combined the assimilation of satellite-derived skin temperatures with the intermittent assimilation of hourly surface observations to study circulations forced by cloud shading.

The objective of this study is to demonstrate the feasibility of a new technique that allows continuous assimilation of surface observations to improve boundary-layer predictions. For this purpose, we performed numerical simulations using a 1D ABL model. We hypothesize that simulation errors in the ABL can be reduced if the measured or analyzed temperature and moisture data in the surface layer can be assimilated in a way that minimizes the disruption of the model's physical processes within the ABL. To this end, we focus on the corrective measures based on the surface-layer data at the ground surface, which in turn exerts a dominant control on the natural evolution of the ABL, while also retaining direct assimilation of these data in the surface layer. The research cited above has shown that simultaneous use of surface-layer temperatures and moisture observations can help to overcome uncertainties in the estimation of soil moisture. However, these data should also be useful for correcting spurious effects due to possible errors in the simulated cloud shading and other sources of model errors affecting the surface layer. We believe that in some cases errors in the simulated surface-layer variables may not be due solely to errors in the soil parameters, and therefore we do not insist that the surface fluxes match observed fluxes, given that the goal is to obtain the correct atmospheric structure.

2. Model description

The 1D model of Alapaty et al. (1997a) has been adopted in this study. It uses advanced local and nonlocal boundary layer formulations to represent turbulent processes of the ABL realistically with an efficiency suitable for three-dimensional (3D) models. For this study the model is configured with 35 vertical layers from the surface to the top at about 5000-m altitude. The lowest layer is about 20 m in depth, placing the first calculation level at about 10 m. There are 18 layers below 850 hPa, with about 80-m resolution in the ABL, which is typical for many mesoscale models. The 1D model predicts the wind (eastward and northward components), temperature, and mixing ratio of water vapor and provides the option to specify externally the horizontal advection and effects of other three-dimensional dynamical processes on the prognostic variables. The user can select from various turbulence schemes and soil–vegetation interaction formulations; however, we describe below only the physical parameterization schemes that were used in this study.

To represent the surface latent heat fluxes, we have chosen a simple formulation, suggested by Carlson and Boland (1978). It contains prognostic equations for temperature in two soil layers, representing surface and subsurface processes; the first layer is 0.01 m thick and the second is 1 m thick. Net radiation at the surface is calculated as the sum of incoming solar radiation absorbed at the surface, atmospheric longwave backscattering radiation, and outgoing longwave surface radiation (Idso et al. 1975; Pleim and Xiu 1995). Upward and downward longwave radiation are calculated as suggested by Grell et al. (1994), as functions of soil emissivity, ground temperature, atmospheric longwave emissivity, and atmospheric temperatures. The lower part of the ABL (i.e., surface layer) is parameterized based on similarity theory suggested by Monin and Yaglom (1971) using the nondimensional stability parameters Φ_m, Φ_h, and Φ_q for momentum, heat, and moisture, respectively. In this study, we used a combination of an asymmetric convective model (a nonlocal closure model) for convectively unstable conditions (Pleim and Chang 1992) and a local *K*-theory scheme for neutral and stable conditions (Pleim and Xiu 1995; Alapaty et al. 1997a).

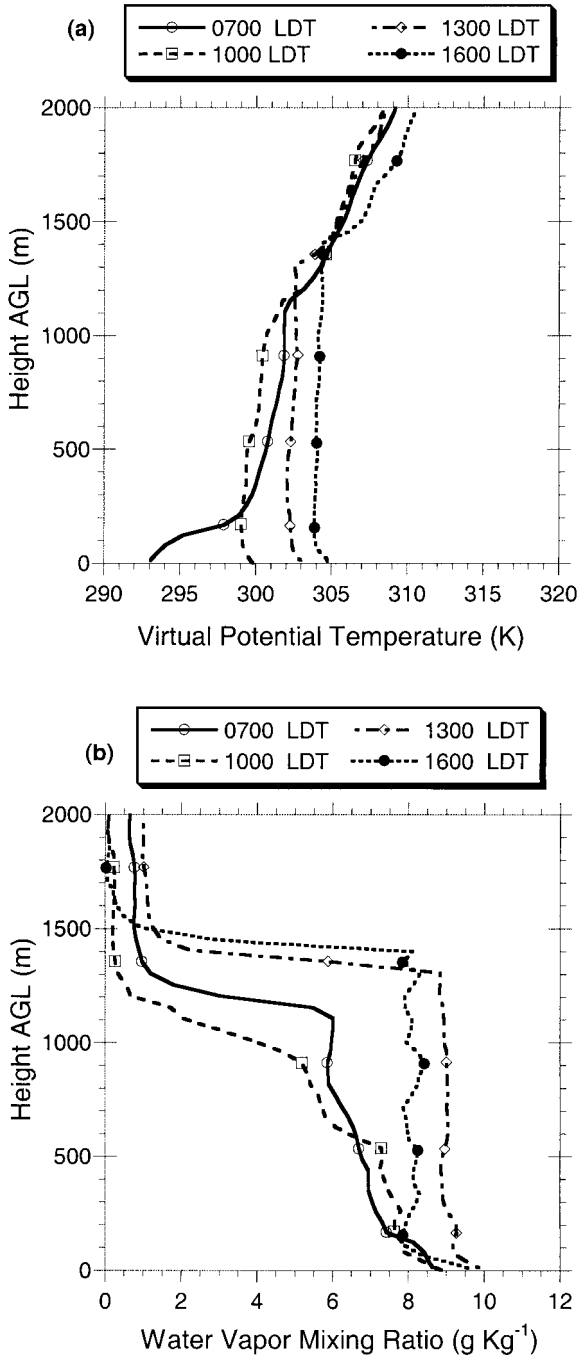

FIG. 1. Observed profiles at Manhattan, KS, for 6 Jun 1987 during FIFE: (a) virtual potential temperature (K) and (b) water vapor mixing ratio (g kg^{-1}). All times in legends are LDT.

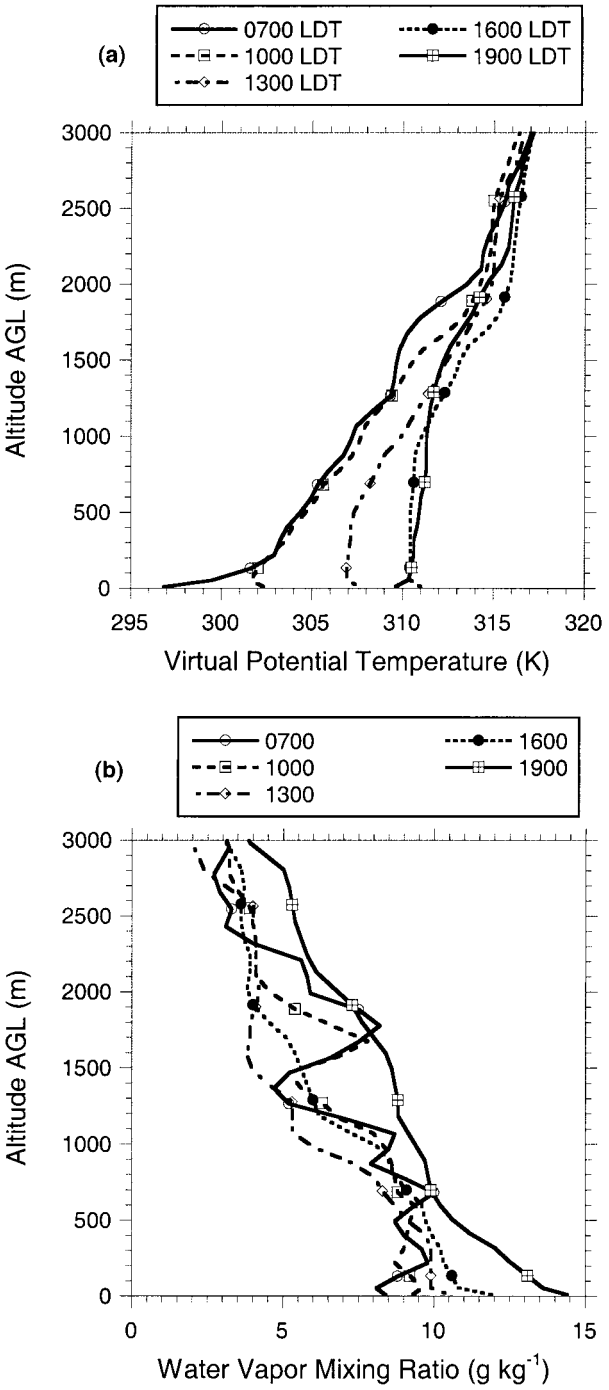

FIG. 2. Same as Fig. 1 but at Buttonwillow, CA, for 3 Aug 1990 during SJVAQS.

3. Analysis of observational data and experiment design

Two cases were chosen for numerical experimentation in this study. The first case was selected from the 1987 First International Satellite Land Surface Climatology Project Field Experiment (FIFE; Sellers et al. 1992), which took place in the relatively flat tall-grass prairie covering a 15 km × 15-km area near Manhattan, Kansas, (39°0′58″N, 96°32′20″W). The second was taken from the 1990 San Joaquin Valley Air Quality Study (SJVAQS) conducted in the complex terrain of central California (Blumenthal et al. 1993). From SJVAQS, we focused on the site at Buttonwillow, California, near

35°24′47″N, 119°28′20″W in the southern end of the San Joaquin Valley.

a. Analysis of FIFE data

In many field studies, including the FIFE program, special observations of the ABL are made mostly during periods when large-scale atmospheric processes are expected to have only weak influence on the evolution of the ABL. The case of 6 June 1987 during FIFE was such a period, during which skies were clear, horizontal gradients were weak, and turbulent mixing processes were the dominant mechanisms responsible for ABL growth. Single-site radiosonde profiles were used to estimate the geostrophic wind for the 1D model. The availability of special three-hourly radiosondes for winds, temperatures, and water vapor mixing ratio, and hourly surface-flux measurements help to make this case suitable for detailed numerical investigations, and the ABL structure has been simulated successfully by Alapaty et al. (1997b) using 1D models.

Figure 1 shows the measured vertical profiles of virtual potential temperature and water vapor mixing ratio at 0700, 1000, 1300, and 1600 local daylight time (LDT). At 0700 LDT (initial conditions) on this day, the radiosonde observations indicate that the remnants of a nocturnal low-level jet (LLJ) were located about 500 m above ground level (AGL; Alapaty et al. 1997a). Above the shallow nocturnal inversion (~200 m deep), the water vapor mixing ratio q_v had only a very weak vertical gradient at this time, up to ~1150 m, indicating that intermittent turbulent mixing may have occurred because of the shear associated with the nocturnal LLJ (Fig. 1b). However, above the nocturnal surface inversion, the virtual potential temperature θ_v had returned to a somewhat stable profile by 0700 LDT, particularly below 900 m AGL. Subsequent observations through the day reveal that the remnant of the LLJ dissipated as the mixed-layer depth grew, leading to mostly uniform winds within the daytime ABL (not shown). Figure 1 confirms that turbulence in the convectively unstable ABL led to well-mixed conditions for the θ_v and q_v profiles as well. A more detailed description of this case can be found in the literature (e.g., Alapaty et al. 1997a,b).

b. Analysis of SJVAQS data

The second site, at Buttonwillow, is located in the southwestern part of the San Joaquin Valley only about 15 km from the innermost Coast Range Mountains. We selected the case of 3 August 1990, when there were few clouds and a quasi-stationary upper-level ridge dominated the synoptic scales (Seaman et al. 1995). Although the site is on mostly flat agricultural and grazing land, the proximity of the Coast Range and Sierra Nevada tends to induce thermally driven mesoscale circulations. These diurnal circulations are frequent during summer and were observed extensively during SJVAQS. This particular episode has been studied by Seaman et al. (1995) using a 3D mesoscale numerical model. Because of the mesoscale valley breeze and upper-level pressure ridge, it is expected that this site should experience substantial midlevel subsidence in this case. Thus, the ABL should develop a more complicated structure at Buttonwillow than was found in the FIFE case, presenting a more difficult challenge for testing the surface-data assimilation strategy. The special data for this episode include three-hourly radiosondes for winds, temperatures, and mixing ratio, and standard one-hourly surface data, but no surface flux measurements.

The observed θ_v profile for this case (Fig. 2a) begins with a deep stable layer in the lowest 2 km that does not vary much between 0700 and 1000 LDT, except that the shallow nocturnal surface inversion is eliminated. Notice that the θ_v profile at 1300 LDT indicates warming of the atmosphere from the surface to the 2000-m altitude, even though there is a negligible vertical gradient only up to about 500 m AGL (the approximate top of the ABL[1] at this time). It is likely that the warming in the layers above 500 m is due to adiabatic sinking of the air mass associated with the east Pacific high pressure ridge and the terrain-induced mesoscale circulations. By 1600 LDT, the top of the ABL appears to have grown to about 900 m AGL, as indicated by the θ_v profile. Again, the effect of mesoscale or large-scale processes can be seen in the warming of the 1600 LDT profile farther aloft, although it is weaker than before. By 1900 LDT, the mixed layer has grown to about 1200 m before stabilizing because of sensible heat flux divergence at the surface an hour or so before sunset. It also can be seen that the capping inversion above the convective boundary layer is weak in the afternoon-observed soundings. Vertical variations in q_v (Fig. 2b) indicate, in general, the presence of unmixed profiles in the ABL through much of the observational period. A possible cause for the strong vertical gradient in q_v in the late afternoon may be explained by the wind profiles during that period, when a substantial east–west shear develops (not shown). This is consistent with the easterly low-level valley breeze directed toward the nearby Coast Range Mountains in the afternoon, with a westerly return circulation at about the height of the ridge top.

In summary, the maximum depth of the ABL at Buttonwillow probably reaches about 1200 m during the late afternoon on this day. The temperature is well mixed, but winds (not shown) and mixing-ratio profiles are not. There is warming in the layers above the daytime ABL, especially between 1000 and 1300 LDT, with a weak afternoon capping inversion. It is obvious that simulating these kinds of ABL structures using a

[1] The height of the ABL has been estimated in this study from special slow-ascent radiosonde data, based on the jump of virtual potential temperature at the mixed-layer top.

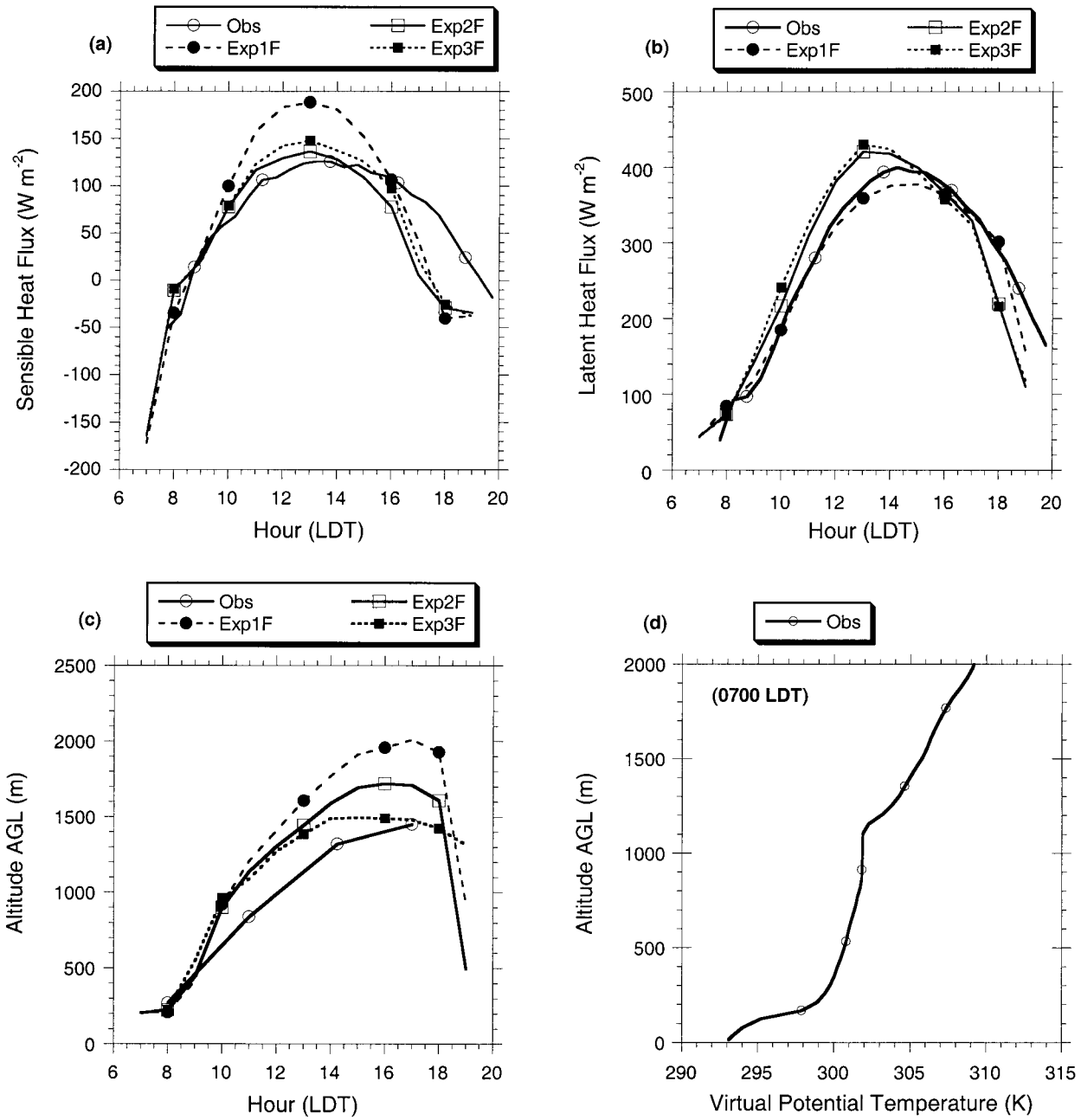

FIG. 3. Observations and model simulations at Manhattan for 6 Jun 1987 during FIFE: (a) surface sensible heat flux (W m^{-2}), (b) surface latent heat flux (W m^{-2}), (c) depth of the ABL (m), and (d) initial (observed) virtual potential temperature (K) at 0700 LDT. Note that for expts 2F and 3F, the surface sensible and latent heat fluxes include the flux adjustments from nudging.

1D model is difficult, but it provides an excellent opportunity to study the impact of surface data assimilation.

c. Experiment design

The 1D model described in section 2 was applied for the two cases discussed above. For both cases, the early-morning soundings from 0700 LDT were linearly interpolated to the model's vertical levels to provide initial conditions for each prognostic variable. The experiments then were run for 13 h to study the evolution of the daytime ABL. We have performed two sets of three experiments using the FIFE and SJVAQS data. First, a baseline experiment (experiment 1) is presented in which no data assimilation was used. In the next experiment (experiment 2), surface data assimilation for temperature and water vapor mixing ratio was added

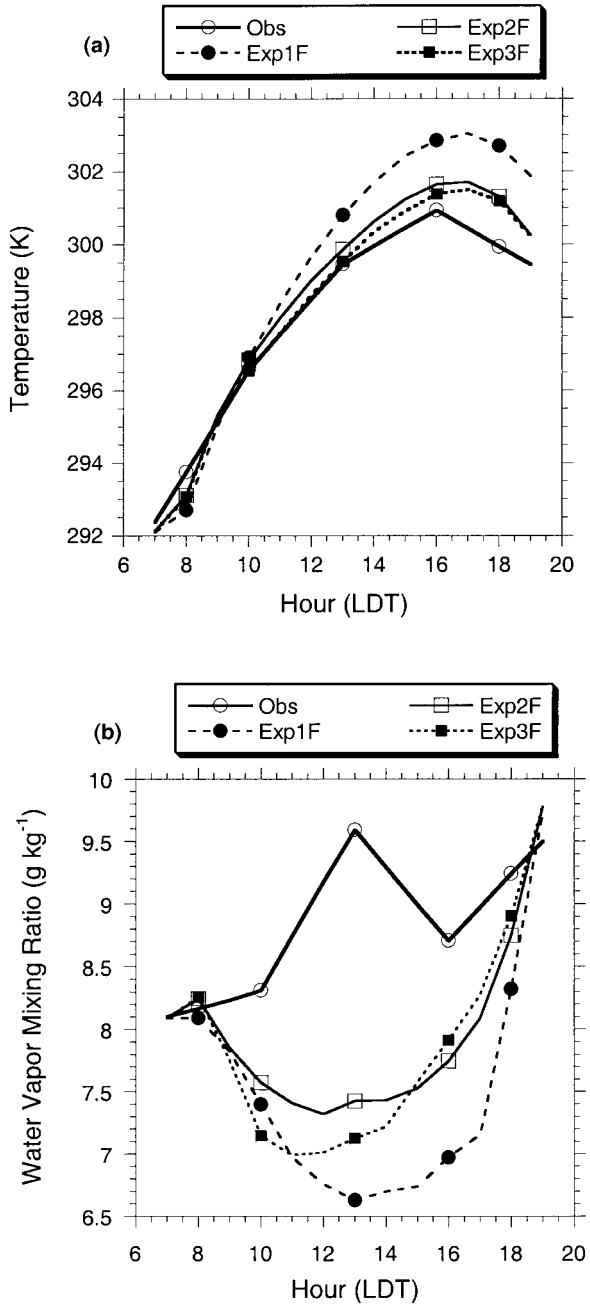

FIG. 4. Observed and model-simulated evolution of the atmospheric surface layer at Manhattan for 6 Jun 1987 during FIFE: (a) surface-layer air temperature (K) and (b) surface-layer water vapor mixing ratio (g kg^{-1}).

using the technique developed in section 4. A third experiment (experiment 3) included the assimilation of the radiosonde-measured wind, temperature, and mixing-ratio data above the ABL in the free atmosphere in addition to assimilating surface temperature and mixing ratio as described for experiment 2. None of the experiments assimilated data within the ABL above the surface layer.

During the model integration in experiment 3, FDDA, based on the Newtonian relaxation method of Stauffer and Seaman (1990) and Seaman et al. (1995), was used to assimilate the special radiosonde data above the ABL by temporally interpolating between the three-hourly upper-air data to the current time step. In effect, this simulates the widely used analysis-nudging approach for 3D models while making use of the more frequent upper-level data available for these two cases. Following Grell et al. (1994), we define the nudging factor for temperature, moisture, and wind as $G = 3.0 \times 10^{-4}$ s^{-1}. By using FDDA to correct for possible model errors in the environment above the ABL that may arise from the absence of 3D processes in the current 1D framework, we indirectly allow for correction of the entrainment fluxes that develop as the ABL grows. No assimilation of the radiosonde data is performed within the ABL, however, so the model solution there depends only on the local turbulence physics and the surface and entrainment fluxes. Details of the new surface data assimilation technique are given in the following section.

4. Surface data assimilation method

To perform surface data assimilation in our 1D model, we have extended the FDDA scheme that was suggested by Stauffer et al. (1991) for assimilating surface-layer data in 3D models (also see section 3). The adaptation of the technique can be developed for a surface variable α starting from the standard 1D nudging equation

$$\partial\alpha/\partial t = F(\alpha, \sigma, t) + G_\alpha(\hat{\alpha} - \alpha), \qquad (1)$$

where α is either the surface temperature T_S or surface mixing ratio q_S, and $\hat{\alpha}$ is the analyzed (gridded) value obtained from observations for α, so that

$$\partial T_S/\partial t = F(T_S, \sigma, t) + G_{T_S}(\hat{T}_S - T_S), \quad \text{and} \qquad (2)$$

$$\partial q_S/\partial t = F(q_S, \sigma, t) + G_{q_S}(\hat{q}_S - q_S). \qquad (3)$$

In (1)–(3), t is time, F is a forcing term representing all physical processes that affect α in the single-column model, and σ is the vertical coordinate. In the case of (2), for example, the physical part of surface temperature forcing, $\partial T_S^P/\partial t$, is

$$F(T_S, \sigma, t) = \frac{\partial T_S^P}{\partial t} = \frac{-(H_1 - H_S)}{\rho C_p \Delta z}, \qquad (4)$$

where H_1 is the heat flux at the top of the lowest atmospheric layer in the model, H_s is the turbulent surface sensible heat flux, ρ is air density, C_p is the specific heat of air at constant pressure, and Δz is the thickness of the lowest model layer. The parameter $G_\alpha = 9.0 \times 10^{-4}$ s^{-1} is the nudging factor that determines the magnitude of the data assimilation term in (1)–(3). Note that the inverse of the nudging factor, $1/G_\alpha$, gives a characteristic assimilation timescale (Stauffer and Seaman 1990). Here, G_α for the surface data is chosen to be 3 times greater than that used for the upper-air sounding data

(see section 3) because the adjustment rate of the surface fluxes to changes in forcing is rapid in comparison with the timescale of the inertia–gravity waves typically responsible for adjustments in the free atmosphere.

The surface assimilation strategy is altered in this methodology to assimilate simultaneously the surface data directly in the lowest atmospheric layer, according to (2) and (3) (Stauffer and Seaman 1990), and also indirectly in the surface energy budget equation for the ground temperature T_g (Grell et al. 1994). This approach maintains consistency in the nudging tendencies at the ground and in the atmospheric surface layer so that the spurious changes in the sign of the surface buoyancy flux noted by Stauffer et al. (1991) are eliminated. To assimilate these observations in the surface energy budget equation, we begin by representing the FDDA terms in (2) and (3), $\partial T_S^F/\partial t = G_{T_S}(\hat{T}_S - T_S)$ and $\partial q_S^F/\partial t = G_{q_S}(\hat{q}_S - q_S)$, respectively, in the form of adjustments to the surface fluxes. The surface-flux adjustments can then be used to change the ground temperature predicted by the model's surface energy budget equation. Note that, in so doing, we do *not* assume that all errors in T_S and q_S are necessarily due to errors in the surface fluxes in every case, and these adjustments should not be considered ''corrections'' to those fluxes. We merely recognize that altering the ground temperature through an adjustment to the surface fluxes based on known errors in T_S and q_S yields a physically convenient indirect way to correct for these errors, regardless of their source.

The proposed adjustment of the ground/skin temperature via the assimilation of the surface data can be completed as follows. First, we can rewrite $(\partial T_S^F/\partial t)\,\Delta t$, the change of the surface-layer (hereinafter the model's lowest layer close to the ground is referred to as the surface layer) temperature in the time interval Δt due to the direct nudging, using the same form as in (4). However, because we have chosen to let all of the effect from the data assimilation occur at the surface, then the nudging adjustment to the turbulent sensible heat flux H_S^F (W m^{-2}) can be written as

$$H_S^F = \rho C_p\left[\left(\frac{\partial T_S^F}{\partial t}\right)\Delta t\right]\frac{\Delta z}{\Delta t} = \rho C_p\left(\frac{\partial T_S^F}{\partial t}\right)\Delta z. \qquad (5)$$

Similar, if $\partial q_S^F/\partial t$ is the rate of change of the surface-layer water vapor mixing ratio due to direct nudging, then the adjustment to the turbulent latent heat flux H_l^F (W m^{-2}) can be written as

$$H_l^F = \rho L\left[\left(\frac{\partial q_S^F}{\partial t}\right)\Delta t\right]\frac{\Delta z}{\Delta t} = \rho L\left(\frac{\partial q_S^F}{\partial t}\right)\Delta z, \qquad (6)$$

where L is the latent heat of condensation. Thus, the adjustment to the ground/skin temperature from indirect assimilation of surface-layer temperature and moisture data over the interval $\Delta t(\Delta T_g^F)$ can be written in the form of the surface energy budget equation as

$$\Delta T_g^F = \left(\frac{\partial T_g^F}{\partial t}\right)\Delta t = (H_S^F - H_l^F)\frac{\Delta t}{C_g}, \qquad (7)$$

where C_g is the thermal capacity of the uppermost soil slab per unit area. The ground/skin temperature increment from (7) is applied at the subsequent time step to be consistent with numerical requirements. Note that a positive (negative) adjustment to T_g also can cause a subtle growth (decrease) of the latent heat flux at the surface, in addition to a similar change in the sensible flux, because the latent flux is a function of the surface saturation vapor pressure calculated at T_g (Carlson and Boland 1978). However, this indirect effect on the latent heat flux is small when compared with the direct assimilation of mixing-ratio data in (3). Because it is normal in most 3D models for the turbulence and surface-exchange parameterizations to be written in the form of a 1D column submodel, this procedure can be extended easily to 3D modeling.

To summarize, an advantage of the continuous data assimilation approach used here is that corrections are inserted smoothly at each time step. In an intermittent data assimilation technique, on the other hand, mass and dynamical imbalances can be introduced discontinuously every time the model is restarted with a new analysis, forcing potentially strong adjustments. The intensity of the nudging is based on the current size of the model errors in T_S and q_S and on the magnitude of the factor G_α that controls the typical *e*-folding rate of the assimilation. The value of G_α is chosen so that the artificial terms H_S^F and H_l^F generally remain small in comparison with the physical terms, such as in (4). Although this simultaneous direct and indirect assimilation approach does not ensure that the model's fluxes will always be nudged toward the real fluxes (which may or may not be observed), it does adjust them so that the model's air temperature and humidity must converge toward the observations of those variables. Thus, the fluxes are altered to allow the atmospheric structure to develop in a realistic way, regardless of whether the errors in the simulated air temperature and humidity were caused by imperfect surface characteristics or developed because of other problems such as errors in the predicted cloud cover or advection.

5. Results

We present results from three experiments that were run for a 13-h period beginning at 0700 LDT for each of the two cases described in section 3. First, results from the baseline experiment (experiment 1) are presented in which no data assimilation was used. Then, in the next experiment (experiment 2), surface data assimilation for temperature and water vapor mixing ratio and corresponding adjustment of ground temperature were added using the technique developed in section 4. The third experiment (experiment 3) included the assimilation of the radiosonde-measured wind, tempera-

ture, and mixing-ratio data above the ABL in the free atmosphere, in addition to assimilating surface temperature and mixing ratio as described for experiment 2. Note that none of the experiments assimilated sounding data within the ABL. Experiments at the FIFE site are distinguished by the suffix ''F,'' while those at the SJVAQS site are given the suffix ''S.''

a. The FIFE case

Because the surface nudging strategy includes the calculation of adjustments to the surface fluxes, we begin with Figs. 3a,b, which compare the evolution of the simulated and observed surface sensible and latent heat fluxes for the FIFE case (6 June 1987, Manhattan). Note that the fluxes shown for experiments 2F and 3F include the adjustment terms (i.e., H_S^F and H_l^F) due to indirect nudging to allow comparison with experiment 1F. Also note that the terms H_S^F and H_l^F are used only in (7) and not in any other governing equations. In Fig. 3a, it is evident that the baseline experiment (experiment 1F) overpredicts the maximum observed sensible heat flux ($\sim$125 W m^{-2}) by at least 60 W m^{-2} around 1300 LDT, after which it falls too rapidly, reaching 0 W m^{-2} (radiation sunset) at around 1730 LDT. In experiment 2F (with direct and indirect surface data assimilation only), the overprediction of the maximum sensible flux near midday is reduced to only about 10 W m^{-2}. The large midday improvement found in experiment 2F is reversed temporarily near 1600 LDT, when the rapidly falling sensible flux in experiment 1F happens to intersect the observations on the way to developing a large underprediction in the late afternoon. However, by 1800 LDT, experiment 2F again shows a small improvement in the simulated sensible heat flux relative to experiment 1F. Last, when the radiosonde observations are added through data assimilation above the ABL in experiment 3F, Fig. 3a shows that there is only a modest impact on the surface sensible heat flux, either slightly positive or negative. Of course, assimilation of the upper-level data represents a very indirect source of information affecting the surface fluxes, when compared with the surface-layer data, so the result of experiment 3F in Fig. 3a is consistent with expectations.

The impact on surface latent heat fluxes (Fig. 3b) from assimilating surface-layer temperature and mixing ratio is not as easy to interpret as the effect on sensible heat flux. The three experiments produced comparable results and reasonable agreement with the observations through most of the day. However, Fig. 3b shows a moderate increase in the simulated surface latent heat flux in experiment 2F due to the surface data assimilation, reaching about +60 W m^{-2} at 1300 LDT relative to the observed data. As in the sensible heat flux, addition of radiosonde data in experiment 3F had little impact on the surface latent flux. These results demonstrate that, as anticipated, the indirect surface data assimilation does not always act to reduce model errors in the surface fluxes. That is, the indirect nudging terms (H_S^F and H_l^F) were designed to assimilate observations of surface air temperature and moisture to reduce model errors in these and other *atmospheric* variables. The surface flux adjustments act only to provide a connection to the predictive equation for ground temperature that drives the ABL. The effect on surface-layer temperature and mixing ratio will be examined below.

Figure 3c shows results for the three simulations of ABL depth, and Fig. 3d presents the initial θ_v profile into which the ABL grows. In experiment 1F, the ABL depth is greatly overpredicted in the afternoon, by as much as 575 m (Fig. 3c). Addition of surface data assimilation in experiment 2F reduces the time-averaged mean errors, mean absolute errors, and root-mean-square errors (rmse; Stauffer et al. 1991) for this case by about 40% (see Table 1). In experiment 3F, use of both surface and upper-air data has further reduced the errors in predicted depth significantly and clearly has produced the best result of the three experiments (errors are 62%–69% lower than in experiment 1F). Table 1 also shows that the mean fractional bias MFB decreases from about +23% in experiment 1F to only about +7% in experiment 3F, where MFB is given by

$$\text{MFB} = \frac{\sum_{n=1}^{N} \frac{(M - O)}{O}}{N}, \tag{8}$$

and where M are the model predictions, O are the observations, and N is the total number of observations. Given that the ABL depth is strongly sensitive to both surface fluxes and the entrainment fluxes at the top of the ABL, it is not surprising that both kinds of data assimilation have an important impact in reducing model errors for this important variable.

Figure 4 compares results of experiments 1F–3F with the observations for the surface-layer air temperature and water vapor mixing ratio. Figures 4a,b indicate that the errors of the baseline (experiment 1F) are significantly reduced in experiment 2F for both variables, especially for the surface temperature. Table 1 confirms that rmse for temperature and mixing ratio is decreased by 56% and 22%, respectively, when the surface data are assimilated in experiment 2F. Figure 4b is of note because of the large differences that develop in experiment 1F between the observed and simulated mixing ratios at 1300 LDT. The large errors at midday are due in part to a rapid increase in the observed surface-layer mixing ratio that was completely missed by the baseline model. Moreover, the model's surface mixing ratio is a minimum at this time, probably because of the rapid entrainment of very dry air from aloft as the mixed-layer depth grows (see Fig. 1b). Of course, the surface moisture assimilation in (3) is proportional to the size of the mixing ratio errors. As the errors grow through the morning, the indirect latent heat flux adjustment term H_l^F grows in experiment 2F, causing the response shown

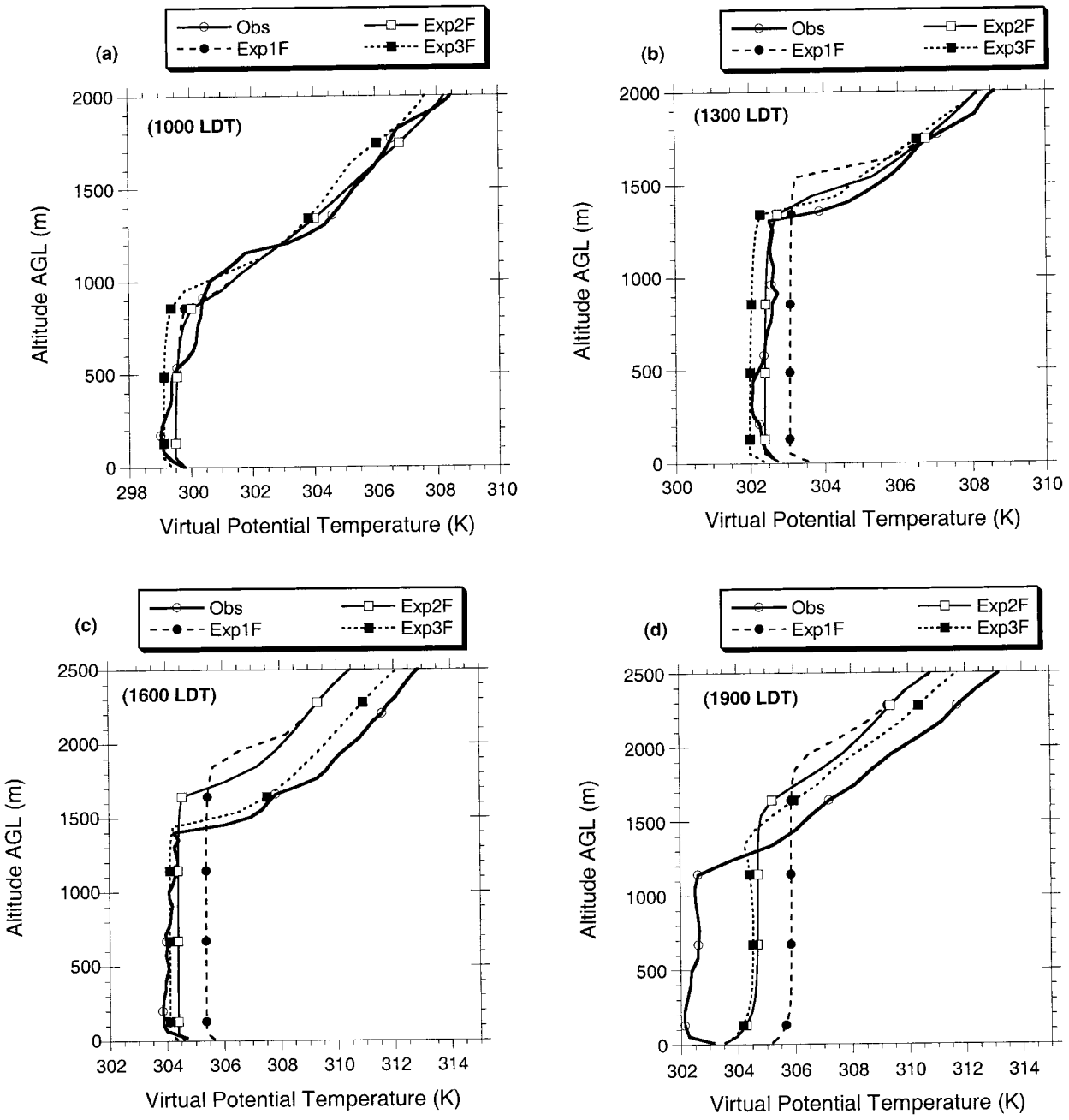

FIG. 5. Observed and model-simulated evolution of virtual potential temperature (K) at Manhattan for 6 Jun 1987 during FIFE: (a) 1000 LDT, (b) 1300 LDT, (c) 1600 LDT, and (d) 1900 LDT.

in Fig. 3b. The impact of H_l^F being greater than 0 is to decrease T_g, as shown in (7), but its indirect effect on the surface-layer mixing ratio (through the saturation vapor pressure at T_g) is small. On the other hand, the direct mixing ratio assimilation in (3) acts to increase strongly the surface-layer moisture (Fig. 4b). In addition, the reduced ABL growth in experiment 2F (see Fig. 3c) results in less entrainment of dry air from above. The net effect of the data assimilation is to moisten the surface layer (and the entire mixed layer). Thus, comparison of Figs. 3b and 4b provides a good example of why the assimilation strategy outlined in section 4 does not attempt to preserve the accuracy of the surface fluxes in all cases. The priority is given to the accuracy of the surface-layer temperature and moisture, which ultimately should have a greater impact on the ABL structure.

Last for the FIFE case, Fig. 5 examines the evolution of the simulated and observed θ_v profiles, following the initial time (also see Fig. 3d). The relationship among

TABLE 1. Statistical evaluation of model results for expts 1F–3F, FIFE case, 6 Jun 1987.

Statistic	Expt 1F	Expt 2F	Expt 3F
	Surface temperature		
Mean error (K)	+1.20	+0.29	+0.50
Mean fractional bias	+0.004 00	+0.001 65	+0.000 97
Mean absolute error (K)	1.43	0.64	0.44
Root-mean-square error (K)	1.66	0.73	0.58
	Surface mixing ratio		
Mean error (g kg^{-1})	−1.36	−1.00	−0.91
Mean fractional bias	−0.150	−0.111	−0.101
Mean absolute error (g kg^{-1})	1.39	1.06	0.96
Root-mean-square error (g kg^{-1})	1.71	1.33	1.19
	Mixed-layer depth		
Mean error (m)	+329.0	+196.3	+102.5
Mean fractional bias	+0.233	+0.143	+0.071
Mean absolute error (m)	359.9	218.8	124.5
Root-mean-square error (m)	404.9	241.1	154.5

the experiments can be seen clearly in Fig. 5c at 1600 LDT. It reveals that both the overprediction of surface temperature and the underprediction of θ_v above the ABL in experiment 1F have contributed to cause the ABL depth to become much too deep. In this case, the assimilation of the surface data via the technique described in section 4 allows the surface-temperature error to be virtually eliminated in experiment 2F. However, because the environment above the inversion is still too cool in experiment 2F, the reduction of error in the ABL depth is less dramatic. When the upper-level sounding data are assimilated above the ABL in experiment 3F, that region warms by up to 3 K at 1600 m AGL, which strengthens the inversion and prevents most of the overprediction in ABL depth. Thus, both kinds of data assimilation work smoothly together to reduce errors in the ABL structure for the FIFE case of 6 June 1987. At 1900 LDT, the observed θ_v profile continues to show a mixed layer up to about 1150 m, while the model has already passed radiation sunset and developed a stable surface layer (Fig. 5d). In a model simulation, stable boundary layer conditions can develop somewhat earlier or later than those in the observations, particularly near radiation sunset. For this reason, during transition times, such as shown in the Fig. 5d, there can be a brief period in the model simulation (several minutes to about an hour) during which the stability profile (convective, neutral, or stable) is different from what is happening in the real atmosphere. However, the surface data assimilation method forces the model's surface-layer (lowest level) predictions toward the observations. In a situation in which the surface observations are becoming colder, the model's stability class may temporarily be opposite (stable) to that of the observed profile (unstable), as shown in Fig. 5d. For a short time, this discrepancy may exist, but it quickly disappears as the real atmosphere also develops a stable profile near the surface shortly after radiation sunset.

b. The SJVAQS case

Figures 6a,b compare the evolution of the simulated surface sensible and latent heat fluxes in experiments 1S–3S for the SJVAQS case (3 August 1990, Buttonwillow). Observed surface fluxes are not available for this case. As for the FIFE case, the surface data assimilation causes midday values of the sensible heat flux in experiment 1S to be reduced by about 60 W m^{-2} in experiment 2S, while the model-estimated latent heat flux (Fig. 6b) shows a growth of about 80–160 W m^{-2} from experiments 1S to 2S. These results suggest that the surface-layer air temperature was overpredicted and the mixing ratio was underpredicted in the baseline experiment (experiment 1S), possibly due in part to an underestimate of the soil moisture in the model. Adding the assimilation of the upper-level data in experiment 3S tended to cause an increase in the surface sensible heat flux on the order of 25–35 W m^{-2} for this case, as compared with experiment 2S, while the latent flux decreased by about 70–100 W m^{-2}.

Figures 6c,d show the development of ABL depth for the three experiments and the initial θ_v profile, respectively. As in the FIFE case, the surface data assimilation at Buttonwillow (experiment 2S) leads to a reduction in ABL-depth errors through most of the day as compared with the baseline run (experiment 1S; Fig. 6c). Table 2 and Fig. 6c show that when the radiosonde data are assimilated above the boundary layer, most of the remaining errors in ABL depth are eliminated, so that for experiment 3S, rmse is 71% less than in experiment 1S. Recall that conditions at Buttonwillow are expected to be more complex than in Kansas because of the proximity to mountainous terrain, so 3D mesoscale and synoptic-scale circulations should lead to substantial subsidence and adiabatic warming aloft. Thus, the large improvement due to assimilating upper-air observations in this case can be attributed in part to the larger model errors above the ABL in the baseline experiment 1S as compared with experiment 1F at Manhattan (see below).

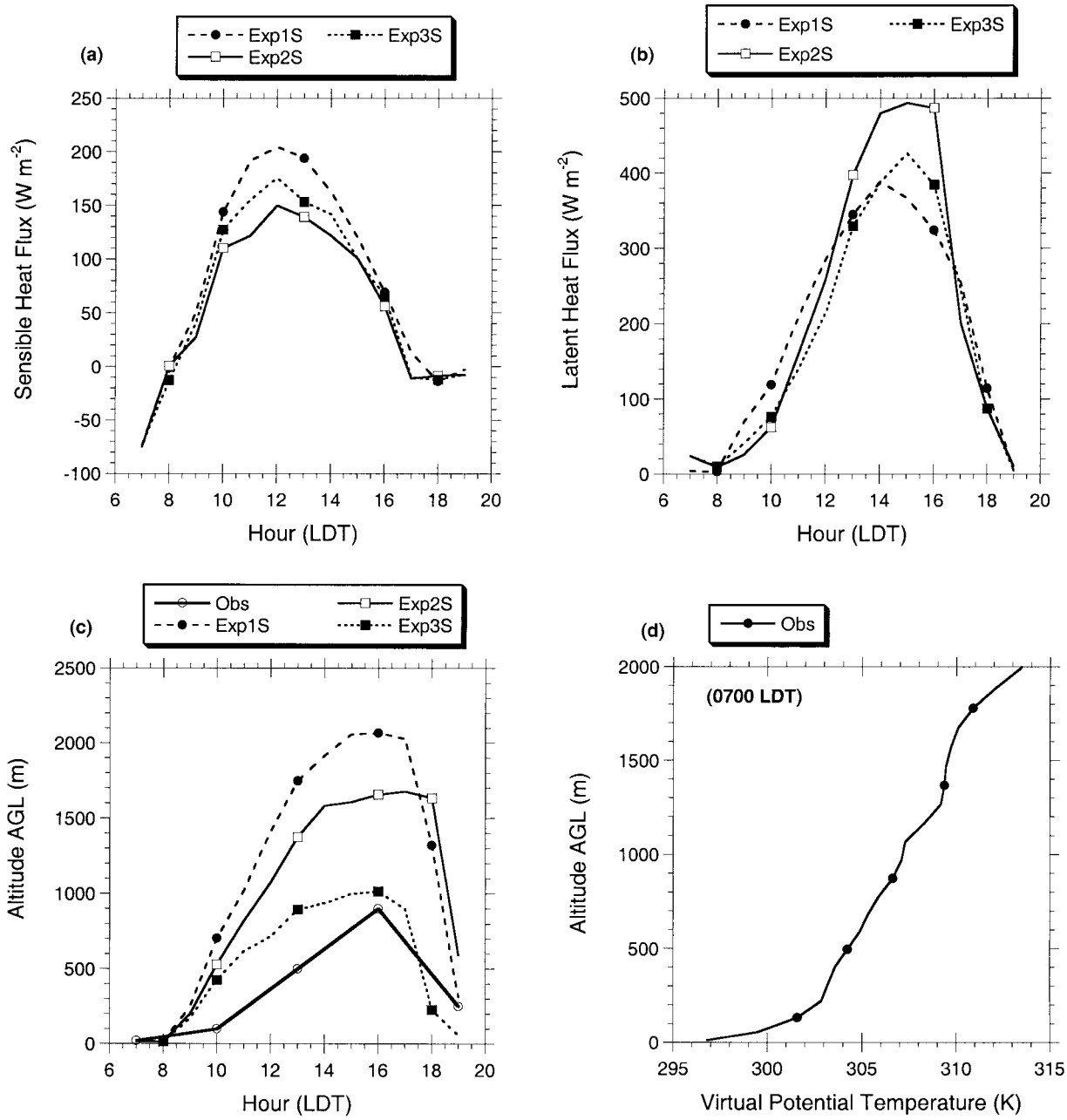

FIG. 6. Model simulations at Buttonwillow for 3 Aug 1990 during SJVAQS: (a) surface sensible heat flux (W m^{-2}), (b) surface latent heat flux (W m^{-2}), (c) depth of the ABL (m; modeled and observed), and (d) initial (observed) virtual potential temperature (K) at 0700 LDT. Note that for expts 2S and 3S, the surface sensible and latent heat fluxes include the flux adjustments from nudging.

The observed and simulated surface air temperatures and mixing ratios at Buttonwillow are presented in Fig. 7. The figure shows that the baseline run (experiment 1S) overpredicts the strong diurnal heating by about 1–2 K and the mixing ratio is underpredicted in the afternoon by about 1.5 g kg^{-1}. The surface data assimilation produces a 63% (55%) reduction of rmse for temperature (mixing ratio) in experiment 2S, with minor additional improvements in experiment 3S (Table 2).

Notice that the response of the surface data assimilation method to the overprediction of temperature found in experiment 1S, as expected, is to reduce the surface sensible heat flux in experiment 2S (see Fig. 6a). Likewise, the response to the underprediction of the mixing ratio in experiment 1S (Fig. 7b) is consistent with results in experiment 2S, for which the mixing ratio becomes greater because of the direct surface-layer assimilation. On the other hand, positive adjustment of

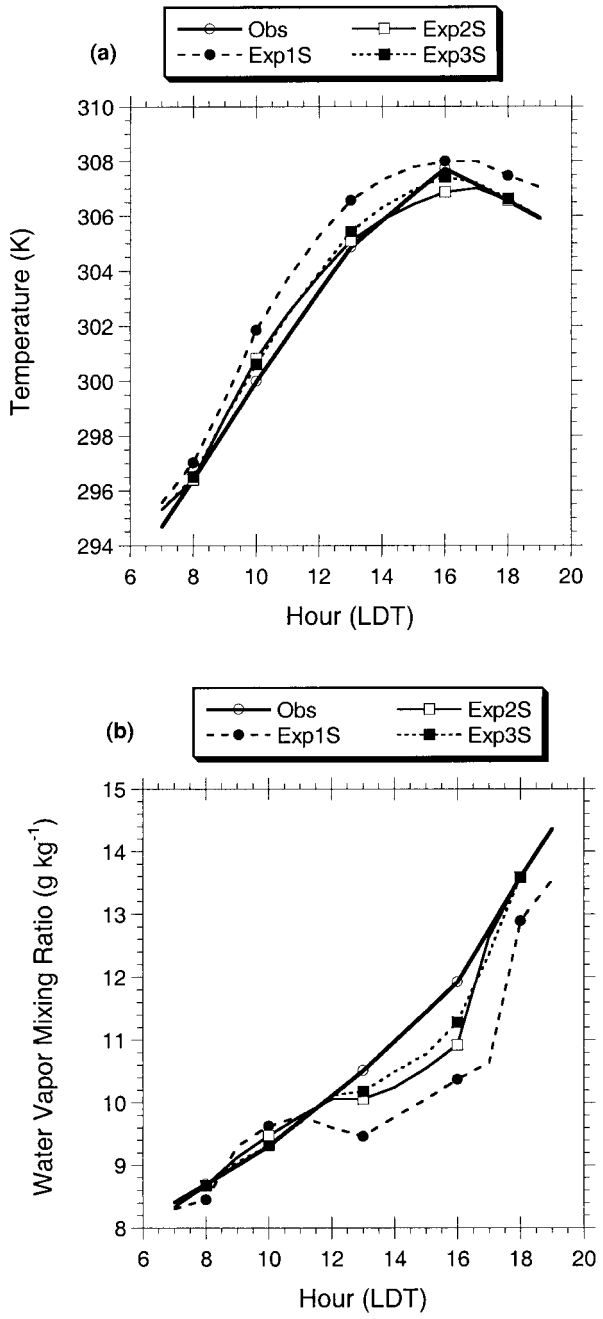

FIG. 7. Observed and model-simulated evolution of the atmospheric surface layer at Buttonwillow for 3 Aug 1990 during SJVAQS: (a) surface-layer air temperature (K) and (b) surface-layer water vapor mixing ratio (g kg^{-1}).

the surface latent heat flux in Fig. 6b via the indirect data assimilation acts primarily to reduce T_g. In addition, this complex response in experiment 2S is aided by reduced entrainment of dry air from above the ABL (not shown). The latter effect occurs because the growth of the simulated mixed layer is slowed in experiment 2S (see Fig. 6c) by the cooler surface temperatures. Thus, we find that the model's physics and the surface data assimilation technique are able to interact in intricate ways when necessary to attain better estimates of the ABL structure.

Last, Fig. 8 shows the evolution of the simulated and observed profiles of θ_v at Buttonwillow. By 1000 LDT, the observed nocturnal inversion (Fig. 6d) had been replaced by a shallow (~100 m) superadiabatic surface layer (Fig. 8a), but the ABL depth had not yet grown appreciably. In the baseline run (experiment 1S), however, the simulated surface air temperature at this time is 2 K too high, causing the ABL depth to grow to about 650 m. Also, notice that the temperatures in the observed profile aloft (above 800 m) have already begun to rise because of the unmodeled 3D processes. (We can compare the observations with experiment 1S in Fig. 8a, because this experiment does not include any data assimilation and the model has no significant physical forcing above the ABL. Thus, at these levels experiment 1S is essentially the same as the observed sounding at 0700 LDT.) Comparison of the experiments in Fig. 8a also shows that assimilation of both surface and upper-level data is important for reducing model errors in the simulated ABL depth. Through the rest of the day, the θ_v errors in experiment 1S continue to grow above the observed ABL, where the atmosphere becomes over 5 K too cool (Figs. 8b–d) and the ABL depth is consistently too deep. The cool upper-level environment occurs because the 3D circulations and subsidence-induced warming aloft are not represented in the 1D model. Notice that the ABL depth had collapsed around 1800 LDT in the model and in the observations because of cooling of the surface layer. This allowed the sounding data to be assimilated and applied down to about 100 m AGL in experiment 3S, which successfully nudged the formerly well-mixed θ_v profile below 1300 m toward the observed stable profile (Fig. 8d). The stabilization above 100 m was caused by continued subsidence and perhaps by differential advection in this part of the column, so experiments 1S and 2S are unable to reproduce this structure.

Once more, these figures demonstrate that both the direct and indirect assimilation of surface data and the direct assimilation of upper-air data are effective for reducing errors in the ABL structure, especially when they are used simultaneously. We also found similar results for the simulated water vapor mixing ratio profiles and the horizontal winds in the ABL (not shown).

6. Conclusions

A 1D ABL model was used to study the impact of assimilating observations of surface air temperature and water vapor mixing ratio for reducing model errors in the ABL. To ensure smooth linkage with the ground characteristics, these data were assimilated both directly and in the form of adjustments to the surface sensible and latent heat fluxes, which in turn were used to in-

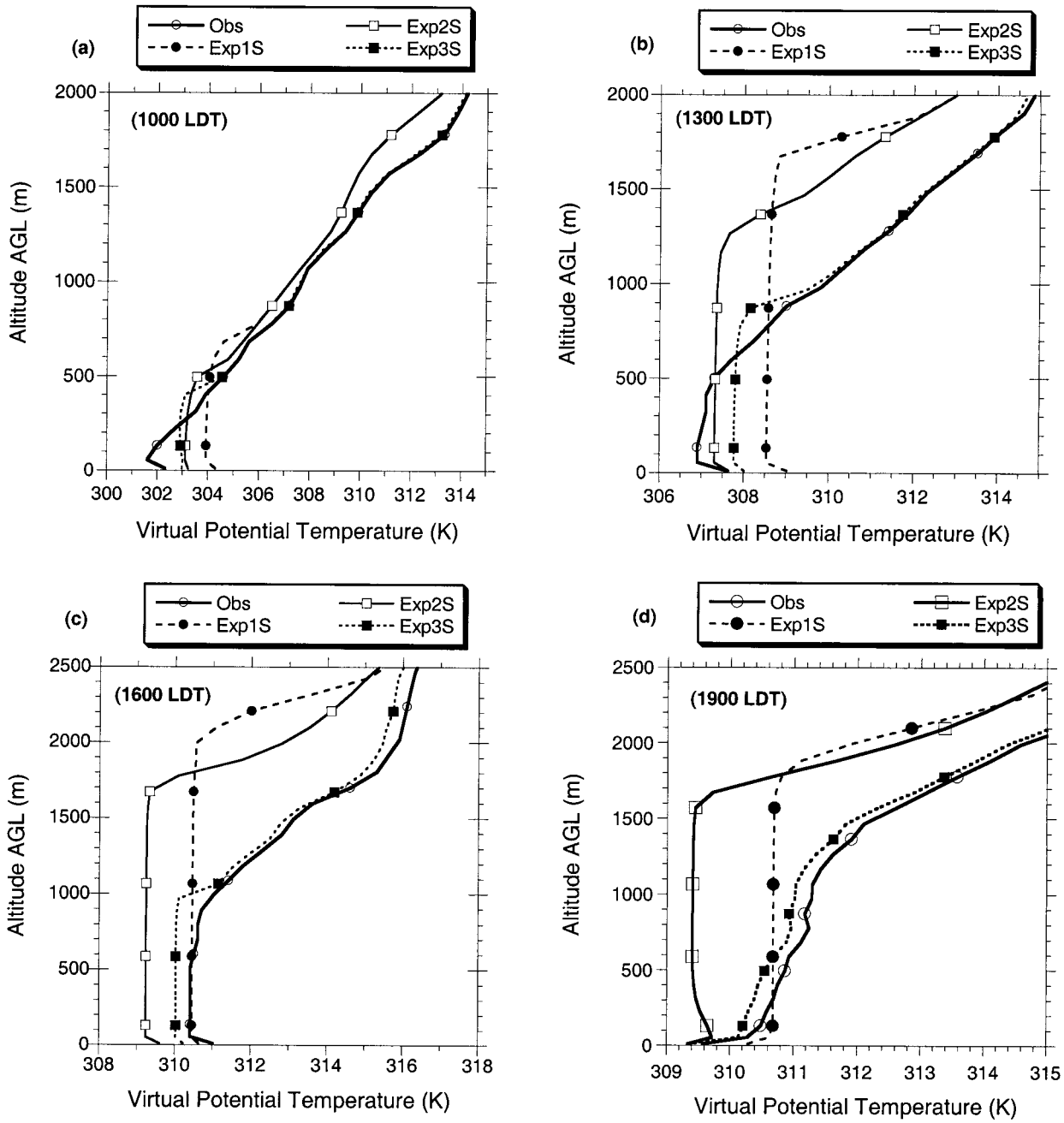

FIG. 8. Observed and model-simulated evolution of virtual potential temperature (K) at Buttonwillow for 3 Aug 1990 during SJVAQS: (a) 1000 LDT, (b) 1300 LDT, (c) 1600 LDT, and (d) 1900 LDT.

crement the predicted ground temperature. This new simultaneously direct and indirect data assimilation technique consistently produced significant improvements in the simulated boundary layer structure, including reduced errors for surface temperature, mixing ratio, and ABL depth. The methodology presented here maintains better consistency between the ground temperature and the surface-layer variables, thereby preventing spurious changes of sign in the model's surface buoyancy flux. The best results were obtained when the surface data assimilation was combined with assimilation of upper-level radiosonde data above the ABL. Even without the three-hourly radiosondes available in these cases, the upper-level data assimilation should remain effective, because tendencies above the ABL generally have a slower timescale than do the forcing terms close to the surface. Meanwhile, the comparatively dense network of hourly surface observations available

TABLE 2. Statistical evaluation of model results for expts 1S–3S, SJVAQS case, 3 Aug 1990.

Statistic	Expt. 1S	Expt. 2S	Expt. 3S
Mean error (K)	+1.23	+0.17	+0.34
Mean fractional bias	+0.004 06	+0.000 59	+0.001 11
Mean absolute error (K)	1.23	0.39	0.38
Root-mean-square error (K)	1.34	0.50	0.46
	Surface mixing ratio		
Mean error (g kg^{-1})	−0.69	−0.23	−0.20
Mean fractional bias	−0.058	−0.020	−0.017
Mean absolute error (g kg^{-1})	0.80	0.29	0.21
Root-mean-square error (g kg^{-1})	1.00	0.45	0.32
	Mixed-layer depth		
Mean error (m)	+753.2	+513.1	+207.5
Mean fractional bias	+2.364	+1.624	+0.952
Mean absolute error (m)	756.9	516.9	211.2
Root-mean-square error (m)	906.5	616.7	263.1

for many continental areas provides a rich database that can be exploited readily using the new technique.

It is simple to adapt this 1D technique for surface data assimilation to a 3D model. There are at least two options available. The first is the analysis-nudging approach of Stauffer and Seaman (1990), in which observations are first analyzed on the model's grid and then assimilated into the model. The second is an observation-nudging approach, in which the data are used in regions of influence extending in both space and time (e.g., Stauffer and Seaman 1994). Analysis nudging is probably more appropriate for assimilating surface data in the new technique described here when there are sufficient data available at the same time to create a reasonably good analysis. Because an objective analysis approach usually does not attempt to fit to all of the data exactly, it tends to filter out some of the nonrepresentative effects due to local siting peculiarities and other data inconsistencies. Observation nudging, on the other hand, is a bit more complex to implement, but it may be a useful alternative for assimilating surface observations when the data are more widely separated in space and time. In either case, however, surface temperature and mixing ratio data can provide a rich source of direct information about the integrated effects that control the surface and entrainment fluxes, including the influences of soil moisture and heat capacity, clouds, advection, and other processes.

The method demonstrated here is suitable for use in a 3D meteorological model and could have favorable implications for a number of data assimilation applications, including the development of improved meteorological fields for air quality modeling. The next step in developing this technique for general use will be its installation and testing in the 3D nonhydrostatic Pennsylvania State University–National Center for Atmospheric Research Fifth-Generation Mesoscale Model.

Acknowledgments. The research reported in this document has been funded by the California Air Resources Board (CARB) under Contract 96-319 to MCNC, and it has been approved for publication by MCNC. The authors thank Mr. Jim Pederson of CARB and the anonymous reviewers for their helpful comments on this manuscript.

REFERENCES

Alapaty, K., and R. Mathur, 1998: Effects of atmospheric boundary layer mixing representations on vertical distribution of passive and reactive tracers. *Meteor. Atmos. Phys.,* **69,** 101–118.

——, J. E. Pleim, S. Raman, D. S. Niyogi, and D. W. Byun, 1997a: Simulation of atmospheric boundary layer processes using local- and nonlocal-closure schemes. *J. Appl. Meteor.,* **36,** 214–233.

——, S. Raman, and D. S. Niyogi, 1997b: Uncertainty in the specification of surface characteristics: A case study of prediction errors in the boundary layer. *Bound.-Layer Meteor.,* **82,** 473–500.

Blumenthal, D. L., and Coauthors,1993: Field program plan for the San Joaquin Valley Air Quality Study (SJVAQS) and the atmospheric utility signatures, predictions, and experiments program. Valley Air Pollution Study Agency Rep. STI-98020-1241-FR.

Bouttier, F., J.-F. Mahfouf, and J. Noilhan, 1993: Sequential assimilation of soil moisture from atmospheric low-level parameters. Part I: Sensitivity and calibration studies. *J. Appl. Meteor.,* **32,** 1335–1351.

Carlson, T. N., and F. E. Boland, 1978: Analysis of urban-rural canopy using a surface heat flux/temperature model. *J. Appl. Meteor.,* **17,** 998–1013.

Chen, F., and J. Dudhia, 2001: Coupling an advanced land surface–hydrology model with the Penn State–NCAR MM5 modeling system. Part I: Model implementation and sensitivity. *Mon. Wea. Rev.,* **129,** 569–585.

——, and Coauthors, 1996: Modeling of land-surface evaporation by four schemes and comparison with FIFE observations. *J. Geophys. Res.,* **101,** 7251–7268.

——, Z. Janjic, and K. Mitchell, 1997: Impact of atmospheric surface layer parameterization in the new land-surface scheme of the NCEP Mesoscale Eta numerical model. *Bound.-Layer Meteor.,* **85,** 391–421.

Grell, G. A., J. Dudhia, and D. R. Stuaffer, 1994: A description of the Fifth-Generation Penn State/NCAR Mesoscale Model (MM5). NCAR Tech. Note TN-398+STR, 138 pp.

Idso, S., R. Jackson, B. Kimball, and F. Nakayama, 1975: The dependence of bare soil albedo on soil water content. *J. Appl. Meteor.,* **14,** 109–113.

Lohmann, U., N. McFarlane, L. Levkov, K. Abdella, and F. Albers, 1999: Comparing different cloud schemes of a single column

model by using mesoscale forcing and nudging technique. *J. Climate,* **12,** 438–461.

Mahfouf, J. F., 1991: Analysis of soil moisture from near-surface parameters: A feasibility study. *J. Appl. Meteor.,* **30,** 1534–1547.

McNider, R. T., A. J. Song, D. M. Casey, P. J. Wetzel, W. L. Crosson, and R. M. Rabin, 1994: Toward a dynamic–thermodynamic assimilation of satellite surface temperature in numerical atmospheric models. *Mon. Wea. Rev.,* **122,** 2784–2803.

Monin, A. S., and A. M. Yaglom, 1971: *Statistical Fluid Mechanics.* Vol. I. MIT Press, 468–504.

Niyogi, D., S. Raman, and K. Alapaty, 1999: Uncertainty in specification of surface characteristics. Part II: Hierarchy of interaction—explicit statistical analysis. *Bound.-Layer Meteor.,* **91,** 341–366.

Noilhan, J., and S. Planton, 1989: A simple parameterization of land surface processes for meteorological models. *Mon. Wea. Rev.,* **117,** 536–549.

Pleim, J. E., and J. S. Chang, 1992: A non-local closure model for vertical mixing in the convective boundary layer. *Atmos. Environ.,* **26A,** 965–981.

——, and A. Xiu, 1995: Development and testing of a surface flux planetary boundary layer model with explicit soil moisture parameterization for applications in mesoscale models. *J. Appl. Meteor.,* **34,** 16–32.

Ruggiero, F. H., K. D. Sashegyi, R. V. Madala, and S. Raman, 1996: The use of surface observations in four-dimensional data assimilation in a mesoscale model. *Mon. Wea. Rev.,* **124,** 1018–1033.

——, G. D. Modica, and A. E. Lipton, 2000: Assimilation of satellite imager data and surface observations to improve analysis of circulations forced by cloud shading contrasts. *Mon. Wea. Rev.,* **128,** 434–448.

Russell, A. G., and R. Dennis, 2000: NARSTO critical review of photochemical models and modeling. *Atmos. Environ.,* **34,** 2283–2324.

Seaman, N. L., 2000: Meteorological modeling for air quality assessments. *Atmos. Environ.,* **34,** 2231–2259.

——, D. R. Stauffer, and A. M. Lario-Gibbs, 1995: A multiscale four-dimensional data assimilation system applied in the San Joaquin Valley during SARMAP. Part I: Modeling design and basic performance characteristics. *J. Appl. Meteor.,* **34,** 1739–1754.

Sellers P. J., F. G. Hall, G. Asrar, D. E. Strebel, and R. E. Murphy. 1992: An overview of the First International Satellite Land Surface Climatology Project (ISLSCP) Field Experiment (FIFE). *J. Geophys. Res.,* **97,** 18 345–18 371.

Sistla, G., N. Zhou, W. Hao, J.-K. Ku, S. T. Rao, R. Bornstein, F. Freedman, and P. Thunis, 1996: Effects of uncertainties in meteorological inputs on Urban Airshed Model predictions and ozone control strategies. *Atmos. Environ.,* **30,** 2011–2025.

Stauffer, D. R., and N. L. Seaman, 1990: Use of four-dimensional data assimilation in a limited area mesoscale model. Part I: Experiments with synoptic-scale data. *Mon. Wea. Rev.,* **118,** 1250–1277.

——, and ——, 1994: Multiscale four-dimensional data assimilation. *J. Appl. Meteor.,* **33,** 416–434.

——, ——, and F. S. Binkowski, 1991: Use of four-dimensional data assimilation in a limited-area mesoscale model. Part II: Effects of data assimilation within the planetary boundary layer. *Mon. Wea. Rev.,* **119,** 734–754.